

VALLEY CIRCULATION EXPERIMENT:
A CLASSIFICATION OF WIND FLOW IN THE
H.J. ANDREWS EXPERIMENTAL FOREST

by

Jerilyn R. Walley

A Thesis
Submitted in partial fulfillment
of the requirements for the degree
Master of Environmental Studies
The Evergreen State College
June 2013

©2013 by Jerilyn R. Walley. All rights reserved.

This Thesis for the Master of Environmental Studies Degree

by

Jerilyn R. Walley

has been approved for

The Evergreen State College

by

Judith Bayard Cushing, Ph.D.

Member of the Faculty

Date

ABSTRACT

Valley Circulation Experiment:
A classification of wind flow in the
H.J. Andrews Experimental Forest

Jerilyn R. Walley

Weak wind flow at night is a poorly understood phenomenon in the field of meteorology. The Valley Circulation Experiment (VALCEX) aimed at creating a wind climatology for the Lookout and McRae Valleys in H. J. Andrew (HJA). Two Sound Detection and Ranging (SoDAR) systems and two sonic anemometers were installed at two stations in adjoining valleys: Lookout Valley, near the HJA Headquarters meteorological station, called Primet, and McRae Valley, approximately 6 kilometers away. Among other variables, each station collected wind speed and direction data in 10 m vertical increments starting at 15 m to 395 m above ground level, aggregated into 5-minute mean averages. Research questions for the study include: 1) To what extent are wind speeds and directions similar at the two stations? 2) Under what conditions do the two instrument locations experience similar phenomena or connectivity? 3) Can a visual classification of sodargrams based on 5 fundamental characteristics in this case synoptic forcing, wind direction, valley jet, pulsing, and similar be used to determine connectivity between the two stations?

Results indicate that based on the 5 criteria the wind flow in the valley was considered connected between the two stations on 43 of the 96 nights classified. The two stations, McRae and Primet, were classified as weak synoptic forcing on 79 of the 96 nights classified. The second criterion, wind direction was classified almost equally at each station; 52 nights were classified as from the North-northeast while 42 nights were classified as from the Southwest. The criterion of valley jet present was determined visually on 49 of the nights..

Keywords: Micrometeorology, Cold-air pooling, SoDAR, Visualization

Table of Contents

Figures.....	v
Tables	v
Acknowledgements.....	vi
1 Introduction.....	1
1.1 The Atmospheric Boundary Layer	3
1.2 Cold Air.....	4
1.3 Valley Jet.....	5
2 Materials and Methods.....	5
2.1 Instrumentation.....	5
2.2 Speed and Directional Computations – Scalar v. Vector	7
2.3 Site Characteristics	9
2.4 Instrument Placement	11
3 Analysis.....	13
3.1 VALCEX and HJA Climate Network Station Data Comparison.....	13
3.2 Sodargram Analysis of 94 days.....	15
3.3 Cases based on classification criteria	23
3.4 Mean wind climatology: March 13 through June 13.....	25
3.5 Case 1 – Weak SF NNE Valley Jet No Pulse Similar	27
3.6 Case 2 – Weak SF SW No Valley Jet Pulse Dissimilar	28
3.7 Case 3 – Weak SF NNE Valley Jet Pulse Similar.....	29
3.8 Case 4 – Weak SF NNE No Valley Jet Pulse Dissimilar (9 nights).....	30
3.9 Case 5 – Weak SF, SW, No Valley Jet, Pulse, Similar (6 Nights).....	31
3.10 Case 6 – Strong SF, SW, No Valley Jet, Pulse, Dissimilar (6 Nights).....	32
3.11 Case 7 – Weak SF, SW, Valley Jet, Pulse, Similar (5 Nights).....	33
3.12 Case 8 – Weak SF, SW, No Valley Jet, No Pulse, Dissimilar (5 Nights)	34
3.13 Case 9 – Weak SF, NNE, Valley Jet, Pulse, Dissimilar (5 Nights).....	35
3.14 Case 10 – Weak SF, SW, Valley Jet, No Pulse, Dissimilar (4 Nights).....	36
3.15 Case 11 – Weak SF, NNE, No Valley Jet, No Pulse, Dissimilar (4 Nights).....	37
4 Discussion.....	38
5 Conclusions.....	41
5.1 VALCEX and HJA Climate Network Station Data Comparison.....	41
5.2 Valley Connectivity.....	42
5.3 Cases based on 5 Classification Criteria	43
6 Future Work & Recommendations.....	43

Figures

Figure 1: SoDAR installed at Primet	6
Figure 2: Cartesian coordinate system X is oriented into the mean wind direction	7
Figure 3: H. J. Andrews Map, Courtesy of H.J. Andrews LTER	10
Figure 4: Topographic map of H.J. Andrews showing SoDAR locations.....	10
Figure 5: Primet location showing surrounding elevations	11
Figure 6: McRae location showing surrounding elevations	12
Figure 7: Distribution of wind speeds of the sonic anemometer and propeller anemometer at Primet.....	14
Figure 8: Comparison of wind speed between the sonic and the cup propeller ...	14
Figure 9: Speed sodargram example.....	16
Figure 10: Directional sodargram example.....	16
Figure 11: Diagram of decision-making process.....	17
Figure 12: Strong Synoptic Forcing classification example.....	19
Figure 13: Weak Synoptic Forcing classification example	19
Figure 14: NNE wind direction classification	20
Figure 15: SW wind direction classification.....	20
Figure 16: Valley jet classification example.....	21
Figure 17: Pulse wind direction classification example	22
Figure 18: Pulse wind speed classification example.....	22
Figure 19: Speed and direction averages by height for study period.....	26
Figure 20: Speed and direction averages by height for Case 1	27
Figure 21: Speed and direction averages by height for Case 2.....	28
Figure 22: Speed and direction averages by height for Case 3.....	29
Figure 23: Speed and direction averages by height for Case 4.....	30
Figure 24: Speed and direction averages by height for Case 5.....	31
Figure 25: Speed and direction averages by height for Case 6.....	32
Figure 26: Speed and direction averages by height for Case 7.....	33
Figure 27: Speed and direction averages by height for Case 8.....	34
Figure 28: Speed and direction averages by height for Case 9.....	35
Figure 29: Speed and direction averages by height for Case 10.....	36
Figure 30: Speed and direction averages by height for Case 11.....	37

Tables

Table 1: Classification Criteria	18
Table 2: Number of Nights by Case	24
Table 3: Number of nights meeting each criterion	39
Table 4: Number of nights meeting each criterion	39
Table 5: Connectivity by Case.....	41

Acknowledgements

It is with immense gratitude that I acknowledge all those who provided me the possibility to complete this thesis. Special appreciation goes to my reader, Dr. Judy Cushing, whose remarks and encouragement throughout this project helped me to complete my thesis, especially during the writing process.

I would like to thank Dr. Christoph Thomas, Oregon State University Biomicrometeorology Group, for introducing me to the field of Micrometeorology, and for so willingly sharing his precious time and equipment. Dr. Thomas conveyed a spirit of adventure in regard to this research and the daunting task of learning MATLAB.

I would like to thank my friends and family who have supported me throughout this project by encouraging me to persevere. I will be forever grateful for your support: Al Walley, Ardith Walley, Craig Walley, Donna Peeples, MJ DeHart, Eryn Farkas and Donna Waters.

VALCEX was supported by Oregon State University Biomicrometeorology Group's Advanced Resolution Canopy Flow Observation (ARCFLO) campaign (NSF Career Award 0955444). Evergreen's Visualizing Terrestrial and Aquatic Systems (VISTAS) (NSF-DBI-1062566) supported my own time on the project.

1 Introduction

The Valley Circulation Experiment (VALCEX) aims at improving the understanding of larger valley-scale airflows in the H.J. Andrews (HJA) Long Term Ecological Research (LTER) Forest. VALCEX goals include determining the vertical structure of airflow dynamics of cold-air drainage in the HJA between Lookout and McRae Valleys. The study analyzed image-based data with a commonly used micrometeorological visualization, the sodargram. This process used visualization to enable insights based on cognitive and perceptual principles by applying human judgment to reach conclusions.

Air exchange between forests and the lower atmosphere plays an important role in transport of heat, moisture, and other trace gasses between the ground and the atmosphere, directly impacting human life and the environment (Thomas et al., 2012). Information about air exchange helps to correctly predict the transport of pollutants and contaminants for various atmospheric conditions and to more precisely estimate carbon sequestration and evapotranspiration rates for tall vegetation. Further, how topography influences weak-wind transport is poorly understood, in spite of the fact that approximately 25% of the earth's surface is mountainous terrain.

Data was collected over an 8-month period using a pair of acoustic ground-based remote sounders installed in two locations within HJA. A SoDAR unit and sonic anemometer were installed at HJA Headquarters in Lookout Valley (dubbed Primet) and McRae Valley (dubbed McRae). Data were analyzed in two

stages. First, data collected from November 30 to December 13, 2011, from the SoDAR and sonic at Primet were compared to a wind cup anemometer that has been collecting data for the past 20 years. Next, data from Primet and McRae were analyzed to determine connectivity within the valley under different mesoscale conditions. The second analysis was completed on 94 days of data, from March 13 through June 23, 2012. This study differs from many micrometeorological studies in its use of visual analytics to classify phenomena (Whiteman et al., 2001; Clements, 2002; Mahrt, 2008; Whiteman and Zhong, 2008; Smith et al., 2009; Dorninger et al., 2011).

Rationale for placing the first installation, Primet, near Headquarters was to compare existing meteorological instrumentation with the SoDAR and sonic, and because of existing infrastructure (power and networking capabilities). Placement of the second installation at McRae Valley was to determine connectivity between Primet and McRae. The McRae installation is north of the confluence of McRae and Lookout Creeks. Wind in the H. J. Andrews was known to flow in two dominant directions, either from the North-northeast, down McRae valley, or from the Southwest, through Lookout Creek valley. The hypothesis was that when wind is from the Southwest, the two locations will experience different phenomena, i.e., be disconnected, and when wind is from the North-northeast, the two stations will show similar speeds and directions, i.e., be connected.

1.1 The Atmospheric Boundary Layer

The Atmospheric Boundary Layer (ABL) is commonly defined as the layer of the atmosphere where the earth's surface influences wind dynamics. The sun heats the earth's surface during the day, which results in an unstably stratified ABL. This in turn results in increasing convectively driven turbulence throughout the ABL. The surface layer is the lowest portion of the ABL and is where the surface fluxes are assumed to be constant with height. The largest area of the ABL is a mixed layer, just above the surface layer, and is generally neutrally stratified. At the top of the ABL is an inversion layer, which separates the ABL from the free troposphere. At night, when net radiation is negative, an inversion layer caps the mixed layer, creating a shallow Stable Boundary Layer (SBL). The SBL grows after sunset due to the earth's surface being colder than the air above. The SBL has generally reduced wind speeds, and wind directions can be subject to sudden shifts of up to 180°, termed "meandering" (Mahrt, 2008). Weak-wind meandering has been studied less than cross-wind fluctuations yet are more directly related to practical problems, such as vertical dispersion of contaminants.

Despite the prevalence of weak-wind conditions, diurnal weak-wind transport is one of the least understood phenomena of micrometeorology (Smoot, 2012). Net radiant energy is the difference between incoming and outgoing components of radiant energy. During the day, heat is transferred from the sun to the earth, creating a surplus of energy at the surface, here defined as positive net radiation; during the night, the net radiant energy is negative. Air in touch with

the ground surfaces gets cooled through conduction and can sink on sloped surfaces because of increased density.

1.2 Cold Air

A cold-air pool is a topographically confined, stagnant layer of air that is colder than the air above (Whiteman et al., 2001). Whiteman et al (2001) characterized cold pools either as diurnal, forming during the evening or night and decaying following sunrise the next day, or as persistent, lasting longer than a normal night-time temperature inversion. In mountainous terrain on a calm clear night, air in contact with the ground becomes cooled from radiative energy loss, and being denser than the warmer air above, sinks to the valley floor (Lundquist et al., 2008). This air can remain stagnant, trapped by the surrounding higher terrain, resulting in long periods of poor air quality and fog, depending on pollution sources and the amount of moisture in the air. With such very weak-wind conditions, wind direction may be quite variable (Mahrt, 2008).

Cold pools begin to form in depressions, valleys, and basins in the early evening when radiant energy is negative. Cold pools can capture moisture, carbon, pollen and pollutants. Pools exchange energy through temperature differences, creating micro currents and turbulence. Cold air drainage requires large-scale wind to be weak, as strong winds will dispel the cold-air pool. According to Mahrt (2010), well-developed cold air drainage has been studied extensively from observations. Whiteman (1990) provides a detailed review of prior studies on cold pooling.

1.3 Valley Jet

A feature of airflow in mountainous terrain is that wind speed increases with height above ground level (agl) more rapidly than it does over level ground. Above a shallow surface shear layer, a low-level jet, a.k.a. valley jet, can form as a vertical band of stronger winds in the lower part of the ABL (Arya, 2001). This requires calm and widely non-turbulent conditions called stable stratification of the ABL; however some intermittent turbulence is almost always present. Under these conditions, a valley jet can occur at 10 to 300 m agl (Folken, 2008). Mayer (2005) defines a low level jet as a thin stream of fast moving air with maximum wind speeds of 10 ms^{-1} to 20 ms^{-1} usually located at 100 to 300 m agl. For this study, I have expanded Mayer's definition of a valley jet to include wind speed occurrences above 3.5 ms^{-1} at 100 to 250 m agl, with lower wind speeds above and below.

2 Materials and Methods

2.1 Instrumentation

The VALCEX study utilized a paired data collection system consisting of a Sound Detection and Ranging (SoDAR) array and a sonic anemometer for data collection (Figure 1). SoDAR is a meteorological instrument and is an acoustic profiler to measure the backscattering of sound pulses for observing wind speed, wind direction, atmospheric turbulence and stability classes. SoDAR systems are used to profile the lower atmosphere from 15 m to $\sim > 1,000$ m agl. VALCEX

used a Meteorologische Messtechnik GmbH (METEK) mono-static phased array acoustic profiler, the PCS.2000-24.



Figure 1: SoDAR installed at Primet

The SoDAR system emits an audible pulse at a defined frequency and listens for the return signal. A small fraction of the energy that travels through the atmosphere is backscattered and received by SoDAR antenna. The scattered elements are small-scale air density variations due to small-scale turbulence in the air column. The return signal intensity and the frequency are processed by the METEK SoDAR to determine wind speed, wind direction, turbulent character of the atmosphere and atmospheric reflectivity at multiple heights (Mayer, 2005; Smoot, 2012). The two SoDARs were programmed to take measurements averaged over 10 m vertical increments, or gates, starting at 15 m and continuing to 395 m agl, depending on atmospheric conditions, at a frequency of 2200 Hz.

Measurements were taken every 8 seconds, then averaged to 5-minute increments by the SoDAR. Smoot (2012) provides comprehensive information on the use of this SoDAR system, SoDAR limitations, fixed echoes and data processing.

Sonic anemometers use ultrasonic sound waves to measure wind speed and turbulence based on the time of flight of sonic pulses between pairs of transducers. The VALCEX sonic anemometer sampled wind speed, wind direction, turbulence and temperature, at the instrument height, at a temporal resolution of 10 Hz, averaging those data to 5-minute and hourly increments. This device collects wind speed and direction using three wind components, with the x-axis aligned to the mean average direction of the wind, the y-axis horizontal and the z-axis vertical with positive upwards (Figure 2).

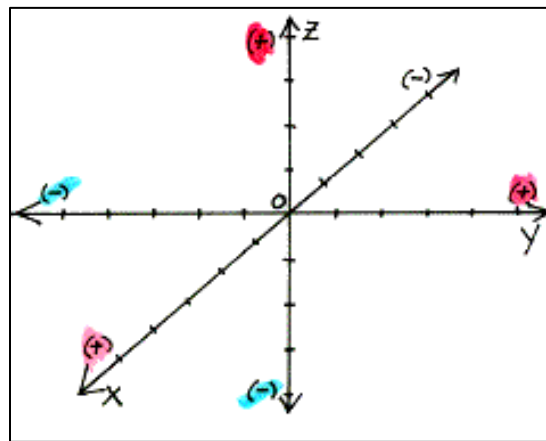


Figure 2: Cartesian coordinate system
X is oriented into the mean wind direction

2.2 Speed and Directional Computations – Scalar v. Vector

Wind has both direction and speed. Both scalar and vector quantities are used to describe wind. Scalar measurements refer to magnitude only, e.g., 27°C .; vector quantities refer to the both magnitude and direction, e.g., 20 ms^{-1} , East.

SoDAR wind speed and direction data are collected using vector averages, i.e., wind components x, y, and z, as shown in Figure 2, are combined to form a wind vector at selected averaging intervals.

Averaging vector quantities differs from averaging scalar quantities since both the vector's direction and magnitude need to be accounted for in the calculation. For example, suppose a constant wind from 360° at 5 ms⁻¹ for 5 minutes changes to 5 ms⁻¹ from 180° for 5 minutes; if vector and scalar averages were calculated for quantities over this 10-minute period, the vector-averaged speed would be zero, whereas the scalar-averaged speed would be 5 ms⁻¹.

In a polar coordinate system, the horizontal wind vector is defined by its mean scalar wind speed (U) and mean horizontal wind direction (ϕ) for each height computed by the SoDAR software as temporal averages over 5 minutes. Temporal variability (σ) over any period with N 5-minute data points is then computed by a MATLAB script as:

$$(1) \sigma_U = \sqrt{\sigma_U^2} = \sqrt{\frac{1}{N-1} \sum_{i=1}^N (U_i - \bar{U})^2}$$

and

$$(2) \sigma_\phi = \Delta\tilde{\phi},$$

with the wind direction difference between subsequent intervals ΔΦ,

which is restricted between 0 and 180°, defined as

$$(3) \Delta\phi_i = \begin{cases} |\phi - \phi_{i+1}| & \text{if } |\Delta\phi| \leq 180^\circ \\ |\phi - \phi_{i+1} - 360| & \text{if } |\Delta\phi| \geq 180^\circ \end{cases}$$

for

$$(4) p(x \leq \tilde{x}) = \frac{1}{2} \text{ and } p(x \geq \tilde{x}) = \frac{1}{2}$$

where p is the probability in the probability density function of the elements of variable x .

2.3 Site Characteristics

HJA is situated in the North-central Oregon Cascades, near the town of Blue River (Figure 3). HJA is a 15,815-acre drainage basin of Lookout and McRae Creeks, which are tributaries of the Blue River, which flows into the McKenzie River. Elevation within the HJA ranges from 410 to 1630 meters above sea level with roughly 1220 m elevation difference between the lowest point, near the headquarters' complex at the southwestern edge, and the highest point at Carpenter Mountain in the northwest corner (Figure 4). McRae Creek flows southeast from its headwaters near Carpenter Mountain toward the Blue River Reservoir. Roswell Ridge rises to an elevation of 1100 m between McRae and Lookout Creeks that flow from the east, joining to become Lookout Creek at 44.233147 N, -122.206421 W, just below VALCEX McRae instrument location.

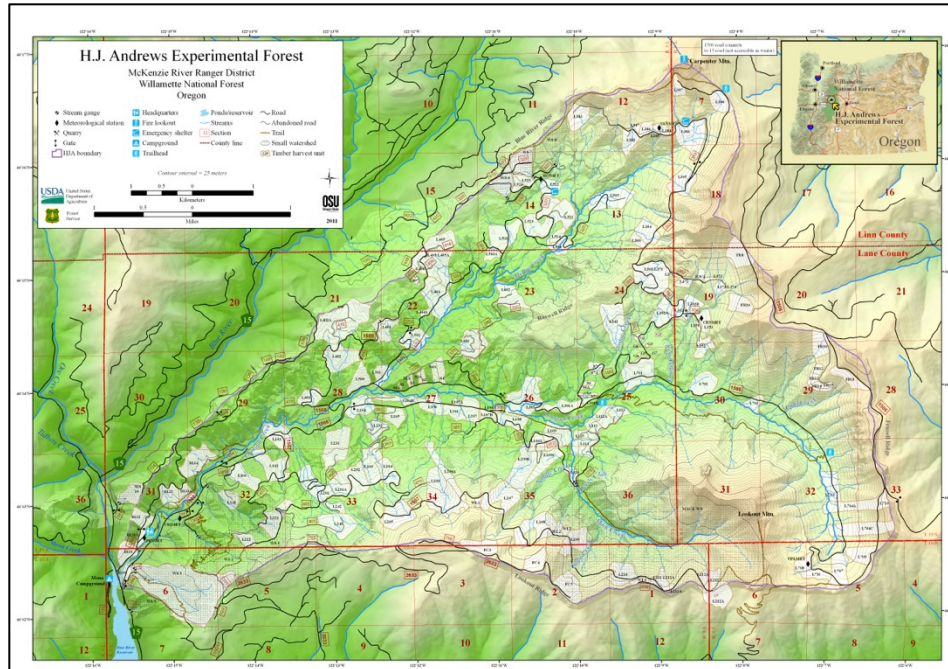


Figure 3: H. J. Andrews Map, Courtesy of H.J. Andrews LTER

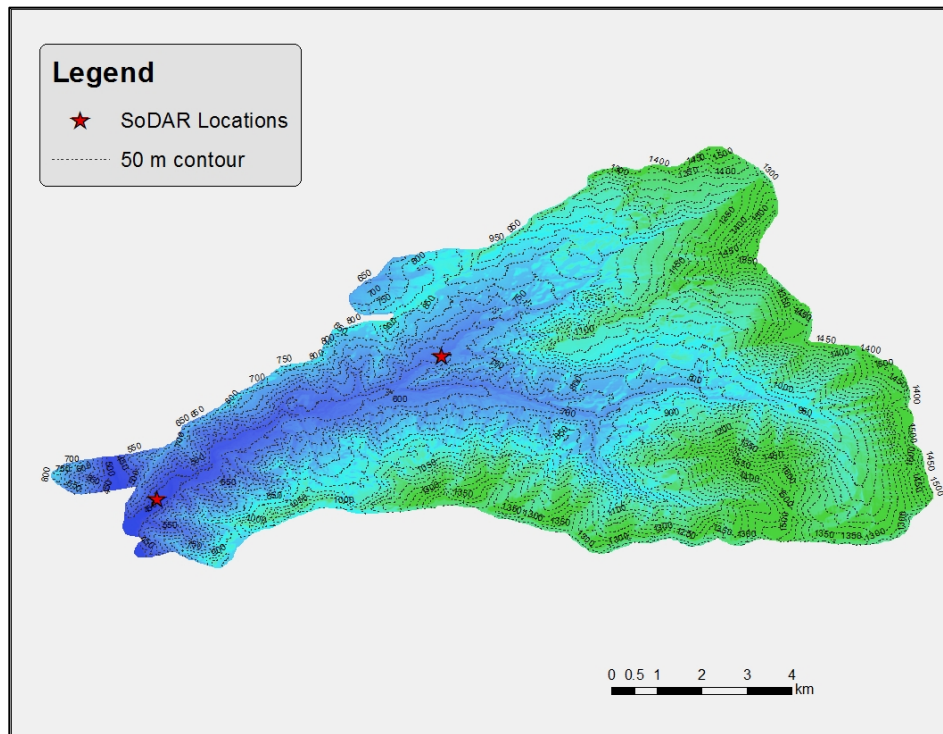


Figure 4: Topographic map of H.J. Andrews showing SoDAR locations

2.4 Instrument Placement

One SoDAR array and one sonic anemometer, referred to as Primet, were installed near the headquarters complex and its meteorological station and situated at 44.211777 North, -122.255954 West, 443 meters (m) above sea level (asl). On October 14, 2011, the SoDAR was installed on a compacted gravel pad with access to electricity and an Internet connection. The sonic anemometer was mounted on an instrumentation tower at 6.81 m above ground level (agl). As shown in Figure 5, this location is at the bottom of Lookout Creek Valley, north of the confluence of Lookout Creek and the Blue River Reservoir. North of Primet is a ridge that runs northwest at an elevation of 600 m to 800 m. To the south is a ridge running east-west which rises to 1,000 meters.

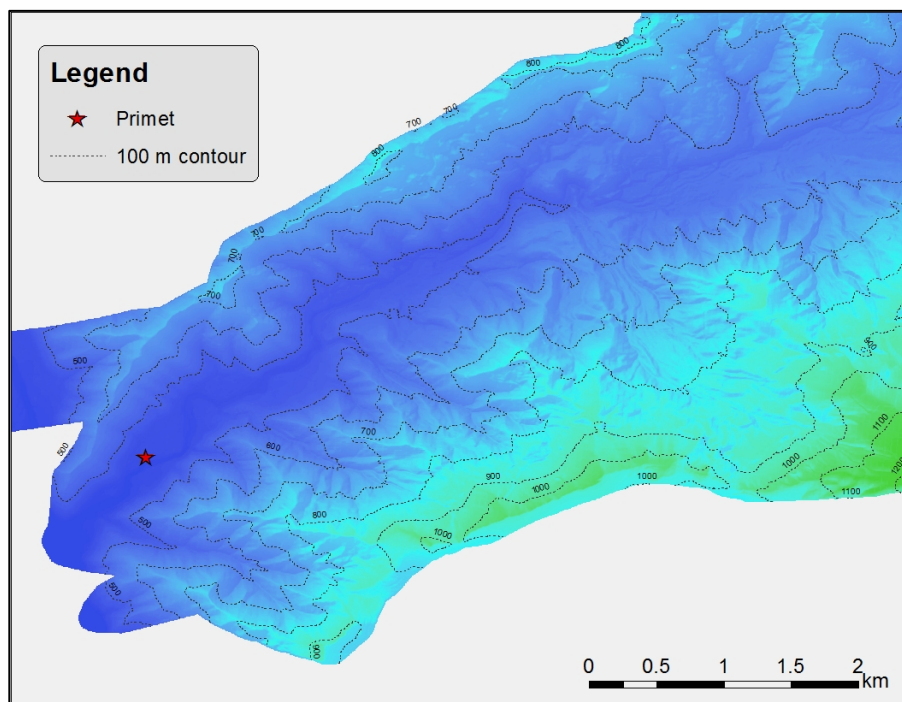


Figure 5: Primet location (44.211777 North, -122.255954 West) showing surrounding elevations

The second SoDAR array was installed October 28, 2011, up McRae Valley at 44. 24037 North, -122.19897 West, elevation 594 m asl. On November 8, the sonic anemometer was relocated to an instrument tower at 6.74 m agl. Due to lack of line power at the McRae Valley site, data collection was limited to the period between 18:00 and 8:00 Pacific Standard Time (PST). On March 12, 2012, a gasoline powered generator to charge batteries was installed that enabled 24-hour data collection. The McRae location is 161 m higher in elevation than Primet. It is nestled in the McRae Creek Valley with a ridge to the south reaching elevations just over 700 m. To the north is the Blue River Ridge that reaches elevations of 1,300 m, turns west and rises to the summit of Carpenter Mountain at 1,630 m, just off the map to the top right in Figure 6. Due west of McRae is Roswell Ridge which climbs to 1,100 m before descending to Lookout Creek.

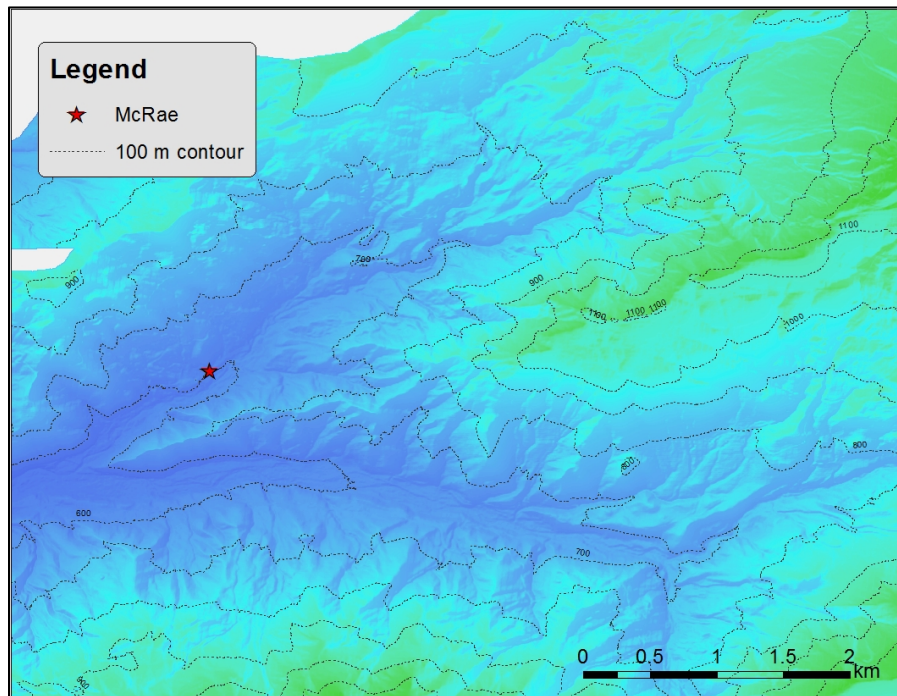


Figure 6: McRae location (44. 24037 North, -122.19897 West) showing surrounding elevations

3 Analysis

3.1 VALCEX and HJA Climate Network Station Data Comparison

Initial analysis focused on validating wind measurements at the HJA existing meteorological climate station, which includes a propeller anemometer. In contrast to the propeller anemometer, a sonic anemometer is thought to be more accurate since it has no moving parts to measure wind speed and direction, and thus has no starting threshold. The motivation was to conduct a feasibility study to determine if VALCEX observations could be extended to the long-term historic data record measured in the HJA. The period of November 30 to December 13, 2011, was selected for comparison because it was dominated by weak, down-valley winds that represent one common mode of the local circulation. Both instruments were mounted at almost the same height (sonic: ~ 8 m agl and propeller: 10 m agl and in close proximity to each other. The comparison between the hourly wind speeds and directions measured with the two different instruments showed that the flows measured with the sonic anemometer were consistently stronger than those observed with the propeller anemometer (Figure 7). The wind speed over the period November 30 to December 13 measured with the sonic anemometer averaged 0.35 ms^{-1} , while that measured by the propeller anemometer was zero, significantly less than the sonic anemometer. The significant scatter in the readings of the propeller anemometer was an additional concern that arose from overspeeding of the sensor during strong gusts and scalar averaging in weak-wind flow characterized by meandering. Wind directions, however, agreed reasonably well with much less scatter between the

two different sensors (Figure 8). We therefore concluded that the historic wind direction data collected from the propeller anemometer is meaningful and can be used to extend the wind climatology, but the wind speeds cannot be used to investigate the strength of the flows.

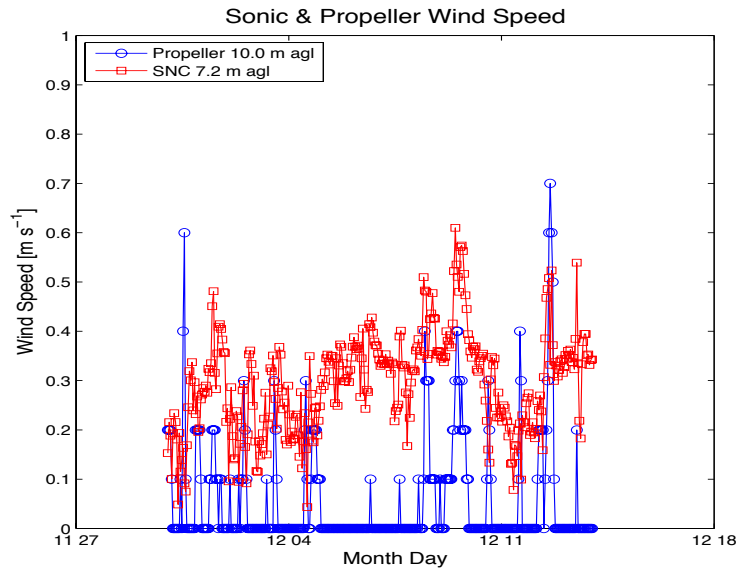


Figure 7: Distribution of wind speeds of the sonic anemometer and propeller anemometer at Primet

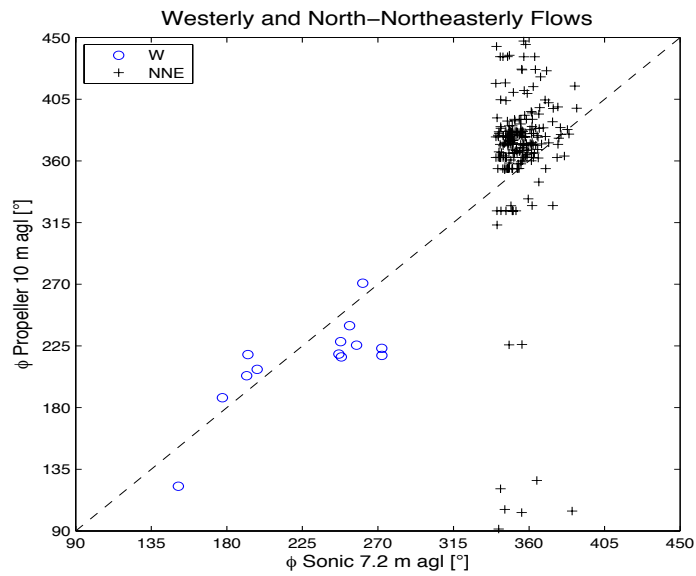


Figure 8: Comparison of wind speed between the sonic and the cup propeller

3.2 Sodargram Analysis of 94 days

This study classified wind speed and direction phenomena for the 94 nights between March 13 and June 23, 2012, through a visual analysis of sodargrams for each 12-hour period centered around midnight. A sodargram is a visual representation of aggregated data for each 5-minute period, with time on the x-axis and each of the 41 gate heights on the Y-axis. The variable of interest is shown by a colored pixel within this 2D coordinate system using a user-defined color legend. Errors and weak signals are visualized in gray. Sodargrams are visualizations commonly used by micrometeorologists; sodargrams for this study were produced using MATLAB. For this study, wind speeds are represented on a scale from black to yellow (Figure 9). Wind direction was represented on a circular scale, with black indicating North, green representing West, blue representing South, and red representing East (Figure 10).

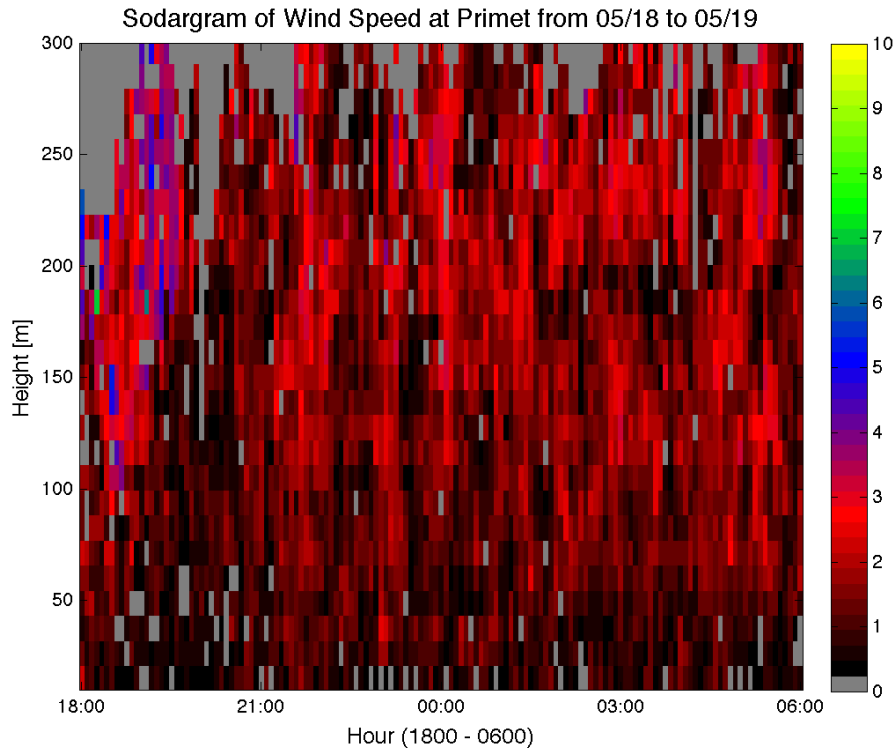


Figure 9: Speed sodargram example

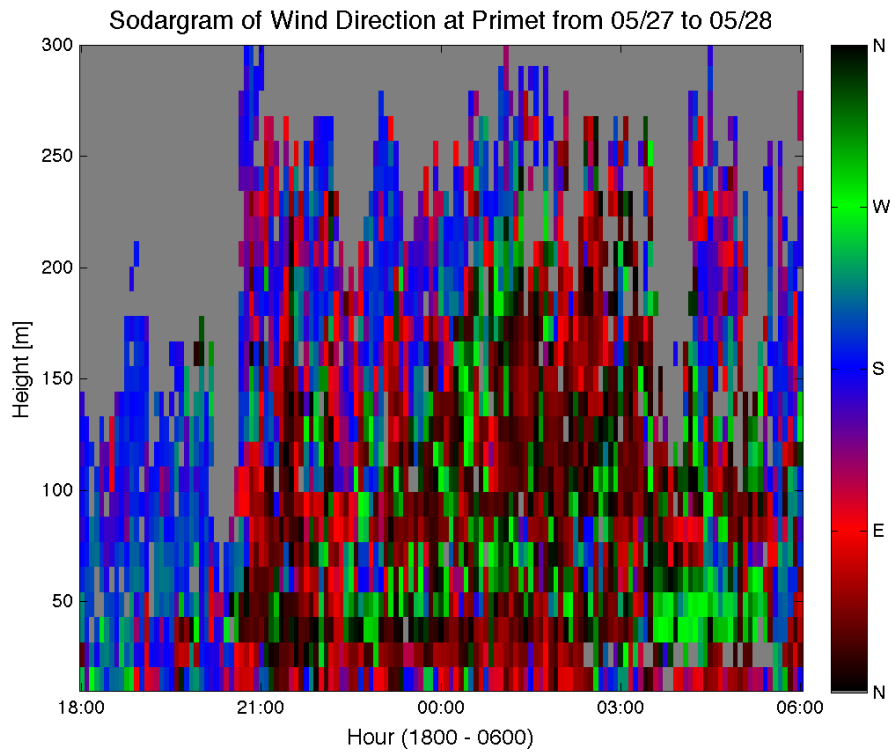
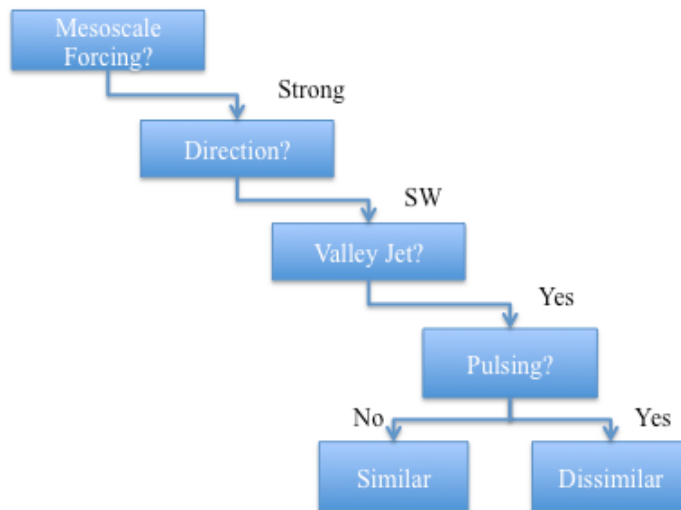


Figure 10: Directional sodargram example
 Note: Color bar indicating black = N on both ends

As cold-air pooling occurs just after the sun has set, when net radiation becomes negative, the classification focused on nighttime phenomena, the period between 18:00 and 06:00. Four sodargrams: Primet Speed and Direction; and McRae Speed and Direction, for each 12-hour period, centered on midnight, were classified visually based on five phenomena (Table 1):

1. Synoptic forcing (Strong or Weak)
2. Wind direction (NNE or SW)
3. Valley jet (Presence/Absence)
4. Pulsing (Presence/Absence)
5. Similar phenomena at both locations (Yes/No)

Each criterion was evaluated independently. The first four phenomena were based on the visual review of Primet and the fifth criterion was based on phenomena at both stations ((Figure 11).



(Figure 11: Diagram of decision-making process.

Table 1: Classification Criteria

Criteria:	Classification		Elevation	Indicator:
Synoptic Forcing	Strong = 1	Weak = 0	50 - 300	Speeds > 5 ms ⁻¹
Direction	NNE = 1	SW = 0	0 – 50	Black & Red (NNE) or Green & Blue (SW)
Valley Jet	Present = 1	Absence = 0	100 – 200	Speeds > 3 ms ⁻¹ with? lower speeds above and below
Pulse	Present = 1	Absent = 0	50 - 100	Pulse of speed and direction
Similar	Similar = 1	Dissimilar = 0	NA	Yes/No

The category of strong or weak synoptic forcing was determined by presence or absence of wind speeds at or above 5 ms⁻¹ for more than 6 hours during a 12-hour period. When wind speeds at or above 5 ms⁻¹ were present, the period was classified as strong (Figure 12). When wind speed remained below 5 ms⁻¹ for the more than 6 hours of the 12-hour period it was classified as weak (Figure 13).

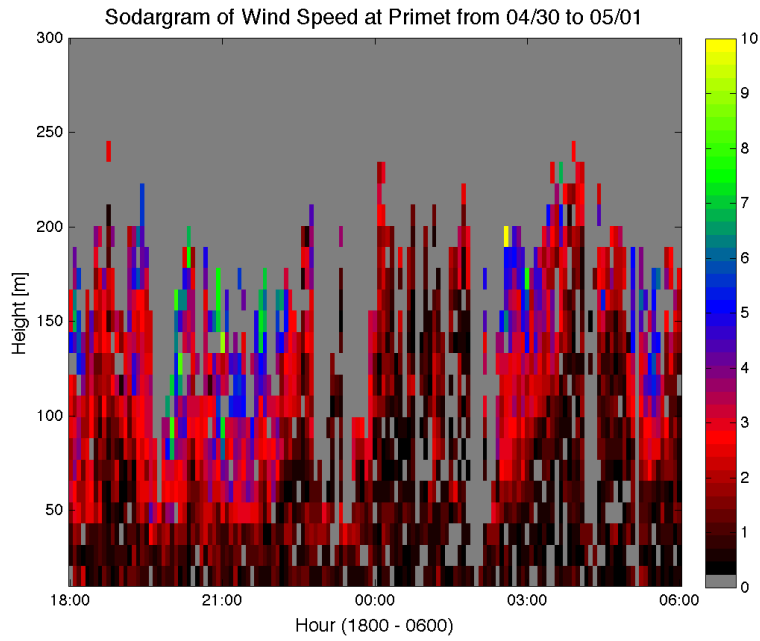


Figure 12: Strong Synoptic Forcing classification example

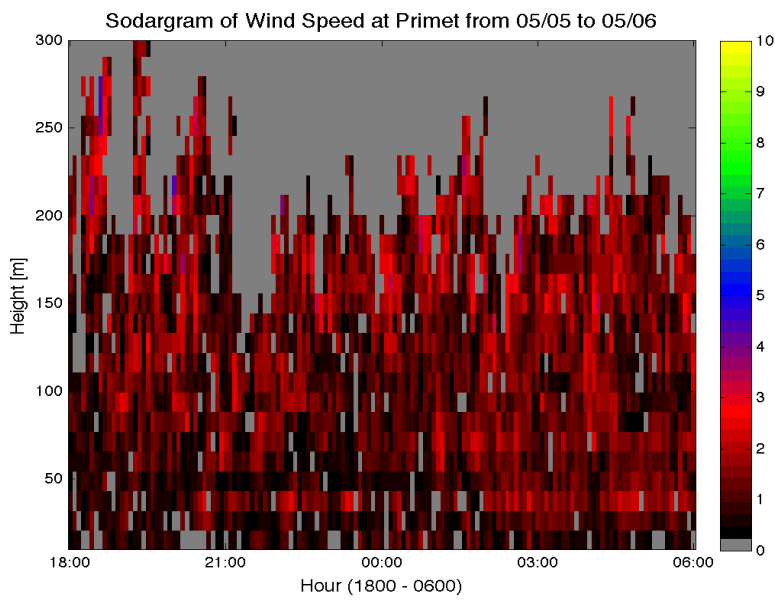


Figure 13: Weak Synoptic Forcing classification example

At low wind speeds, wind direction changes frequently and drastically, as can be seen in Figure 10 on page 16. To determine directional classification for a 12-hour period, heights between 0 and 50 m agl were evaluated to determine the primary flow direction (Figure 14 and Figure 15).

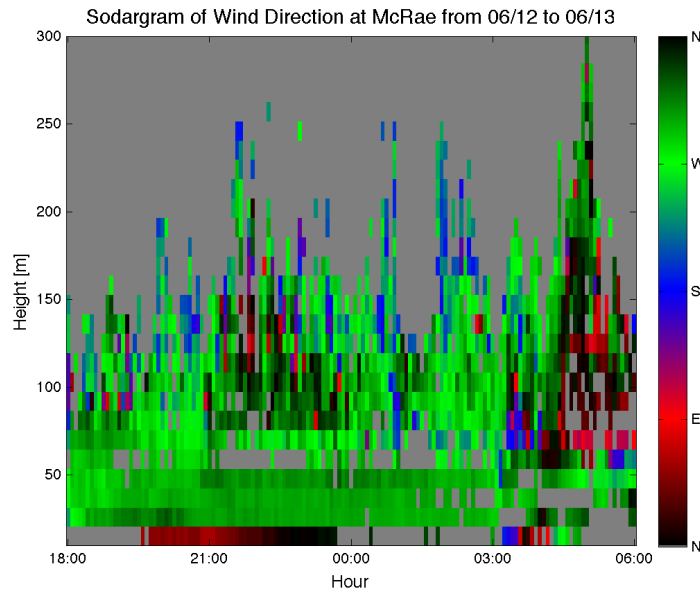


Figure 14: NNE wind direction classification

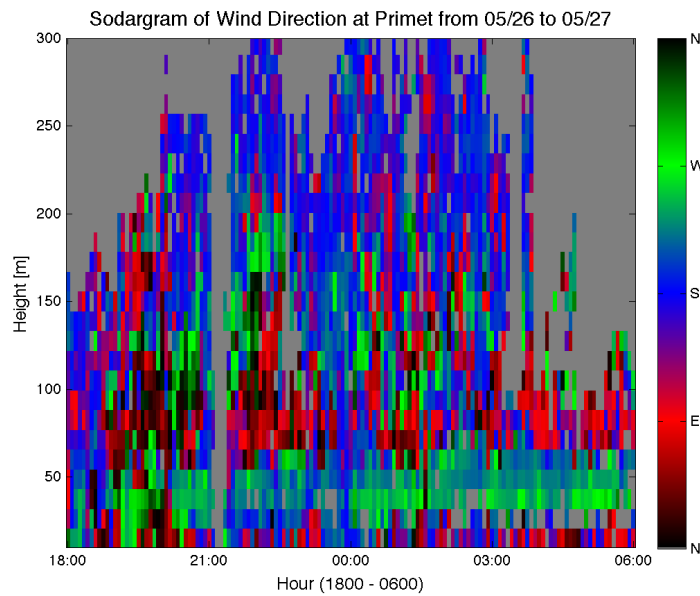


Figure 15: SW wind direction classification

The third classification criterion is the presence or absence of a valley jet, a band of higher wind speed at approximately 100 – 200 m agl. This phenomenon does not fit the classic definition of low-level jet as the speeds are not higher than 10 ms^{-1} . However, as this area is dominated by weak winds, a valley jet was defined as winds at heights of 100 – 250 m agl with slower speeds above and below. The valley jet can be seen as a band of speeds between 2.5 and 4 ms^{-1} , nested between lighter wind speeds, as shown in the circled area on Figure 16.

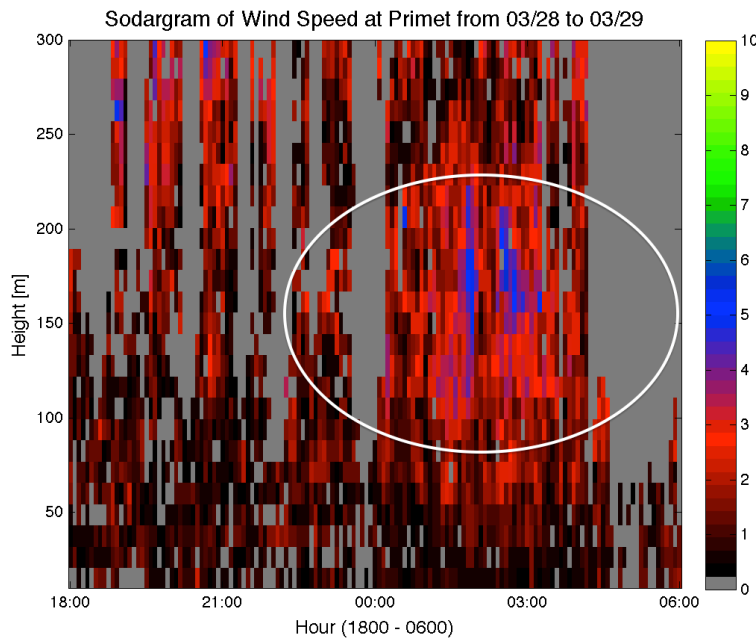


Figure 16: Valley jet classification example (circled)

The fourth phenomenon evaluated was the presence or absence of pulsing, defined as wind directions alternating between 50 and 100 m agl. A pulse typically starts at lower elevations, around 40 m agl, then rises to approximately 100 m agl, and can be seen as a pattern of directional shifts, Figure 17 and Figure 18.

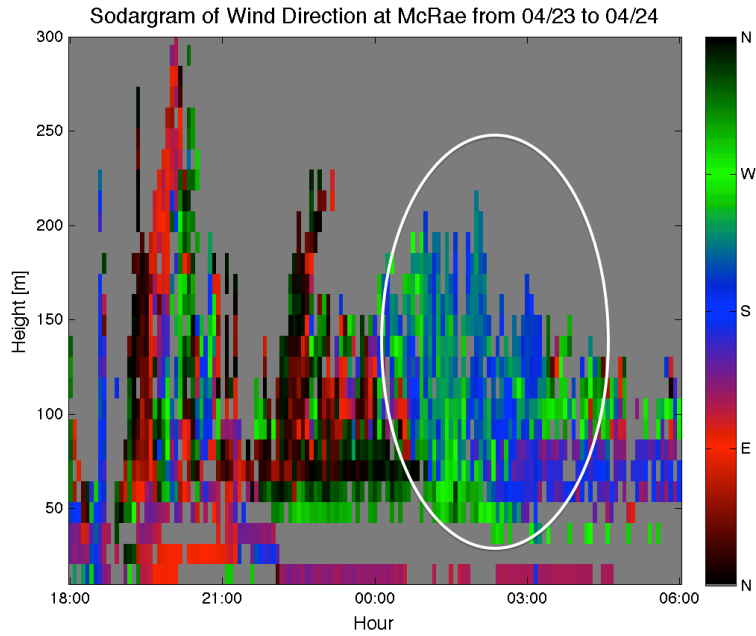


Figure 17: Pulse wind direction classification example (circled)

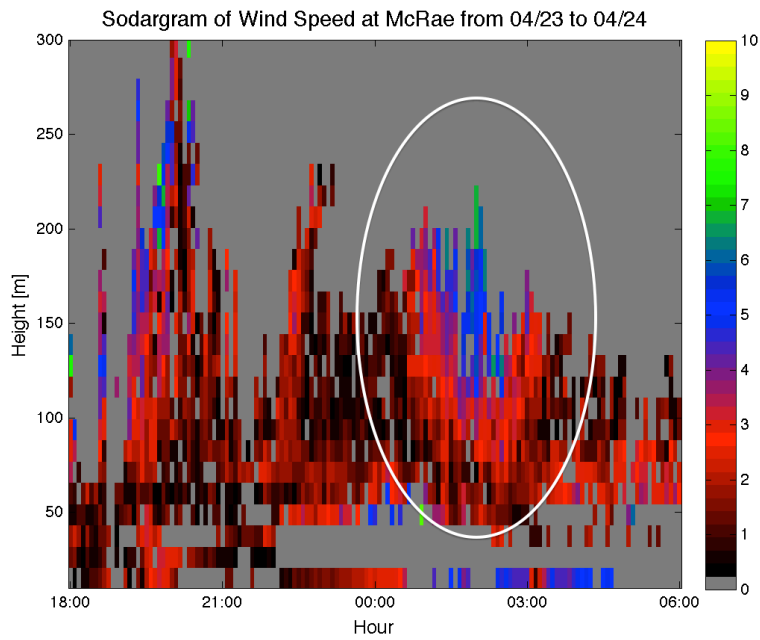


Figure 18: Pulse wind speed classification example (circled)

The final classification criterion was similar or dissimilar. This criterion indicates whether the two locations (McRae, Primet) are similar or dissimilar for wind speed and direction. This criterion evaluates the connectivity within the valley. When evaluating this criterion, all four sodargrams were visually evaluated for similar phenomena for the Synoptic Forcing and Direction criteria.

3.3 Cases based on classification criteria

The 5 classification criteria create 32 potential combinations. The three most commonly observed combinations were:

- Case 1: Weak SF, NNE flows, Valley Jet, No Pulse, Similar (17 nights);
- Case 2: Weak SF, SW flows, No Valley Jet, Pulse Dissimilar (13 nights)
- Case 3: Weak SF, NNE, Valley Jet, Pulse, Similar (12 nights).

Table 2: Number of Nights by Case) shows the 32 possible cases and the number of nights meeting criteria for each case. The cases with 4 or more nights, which comprised 86, or 91% (86 of 94), of the nights classified were analyzed in detail. The 13 cases with only 0 to 3 nights meeting the criteria were not analyzed. These 13 cases comprised only 8 of the 94 nights classified (9%).

For each case analysis, below, it is noted whether wind speed and direction are similar or dissimilar at each location, and whether (and how) those measurements vary with height in m agl. For the nights meeting each case, measurements for wind speed and direction were ensemble-averaged. Graphs for the ensemble-averaged data are included with error bars showing standard deviation, as in Figure 19. It is also noted whether the ensemble averaged speed and direction agreed with the original assessment of similar or dissimilar for each individual night.

Table 2: Number of Nights by Case

Case	Synoptic Forcing	Flow Direction	Valley Jet	Pulse	Similar	Number of Nights	Page Number
1	Weak	NNE	Yes	No	Yes	17	27
2	Weak	SW	No	Yes	No	13	28
3	Weak	NNE	Yes	Yes	Yes	12	29
4	Weak	NNE	No	Yes	No	9	30
5	Weak	SW	No	Yes	Yes	6	31
6	Strong	SW	No	Yes	No	6	32
7	Weak	SW	No	No	No	5	34
8	Weak	SW	Yes	Yes	Yes	5	33
9	Weak	NNE	Yes	Yes	No	5	35
10	Weak	SW	Yes	No	No	4	36
11	Weak	NNE	No	No	No	4	37
12	Weak	NNE	Yes	No	No	3	N/A
13	Strong	NNE	Yes	No	Yes	3	N/A
14	Strong	NNE	No	Yes	Yes	2	N/A
15	Strong	SW	No	No	No	1	N/A
16	Strong	SW	No	No	Yes	1	N/A
17	Strong	SW	No	Yes	Yes	1	N/A
18	Strong	SW	Yes	No	No	1	N/A
19	Strong	SW	Yes	No	Yes	1	N/A
20	Strong	NNE	No	No	No	1	N/A
21	Strong	NNE	No	Yes	No	1	N/A
22	Weak	SW	No	No	Yes	0	N/A
23	Weak	SW	Yes	No	Yes	0	N/A
24	Weak	SW	Yes	Yes	No	0	N/A
25	Weak	NNE	No	No	Yes	0	N/A
26	Weak	NNE	No	Yes	Yes	0	N/A
27	Strong	SW	Yes	Yes	No	0	N/A
28	Strong	SW	No	Yes	Yes	0	N/A
29	Strong	NNE	No	No	Yes	0	N/A
30	Strong	NNE	Yes	No	No	0	N/A
31	Strong	NNE	Yes	Yes	No	0	N/A
32	Strong	NNE	Yes	Yes	Yes	0	N/A

3.4 Mean wind climatology over study period: March 13 through June 13

Wind speed and direction data for all 94 nights between the hours of 18:00 and 06:00 were averaged by gate, i.e., 10 m height increments (Figure 19).

Directional averages between Primet and McRae are dissimilar, starting at Southerly below 100 m agl, diverging above 100 m agl. Directional averages at Primet are 180° at lower heights and shift with height to 90° between 100 and 200 m agl; above 200 m agl directional averages change to 0° . At McRae directional averages at heights between 50 m agl and 100 m agl vary between 180° and 270° ; between 100 and 300 m agl, directional averages are 270° ; above 300 m agl, directional averages vary between $180 - 0^\circ$.

Wind speed averages are similar below 200 m agl at both stations. McRae wind speed averages for the entire period are generally very weak, below 1 ms^{-1} at gates below 195 m agl. Above 205 m agl speed averages increase and are generally greater at the McRae station than at Primet; error bars show variation increasing with elevation. Primet wind speed averages are very weak at all heights. Near zero wind speed variation, shown by error bars, is the result of opposing flows with similar magnitude, so the resultant vector speed is near zero.

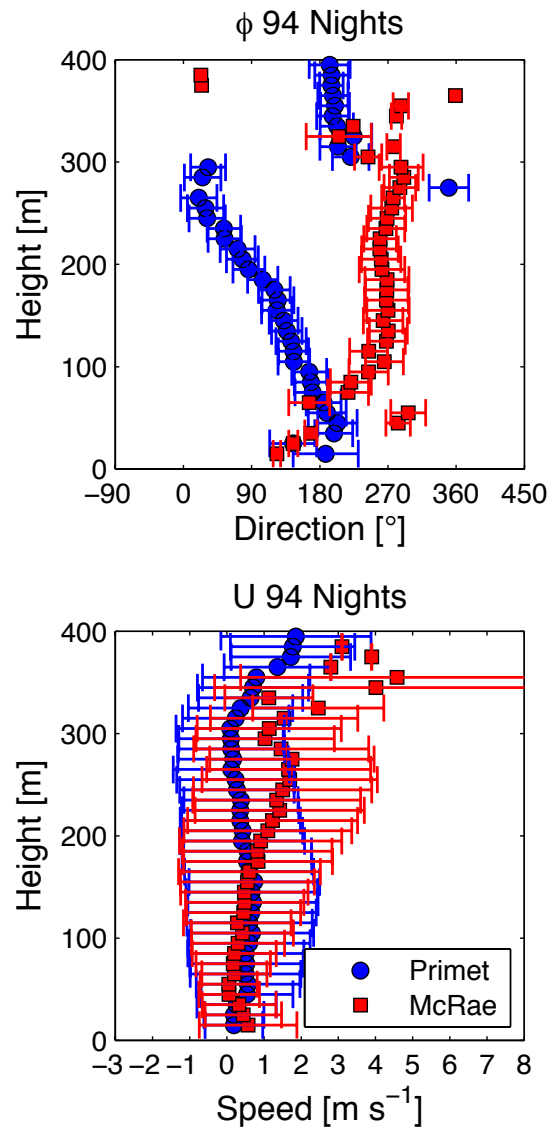


Figure 19: Speed and direction averages by height for study period (94 nights)

3.5 Case 1 – Weak SF NNE Valley Jet No Pulse Similar

Seventeen nights met the classification criteria for Weak SF, NNE flow, Valley Jet, Pulse, Similar. The 17 nights were ensemble-averaged (Figure 20). Wind directional averages for both stations were between 0° and 45° at gates below 195 m agl. Above 205 m, directional averages shift to between 300° and 260° . Both McRae and Primet show similar wind speeds between 0 and 2 ms^{-1} at all heights. McRae has greater average speed variability than Primet between 205 and 305 m agl. The valley jet is weak, with average wind speeds approximately 0.5 m faster between 95 and 165 m agl; this phenomenon can be seen in the sodagram as increased speeds create a slight ‘nose’ between 75 and 105 m agl.

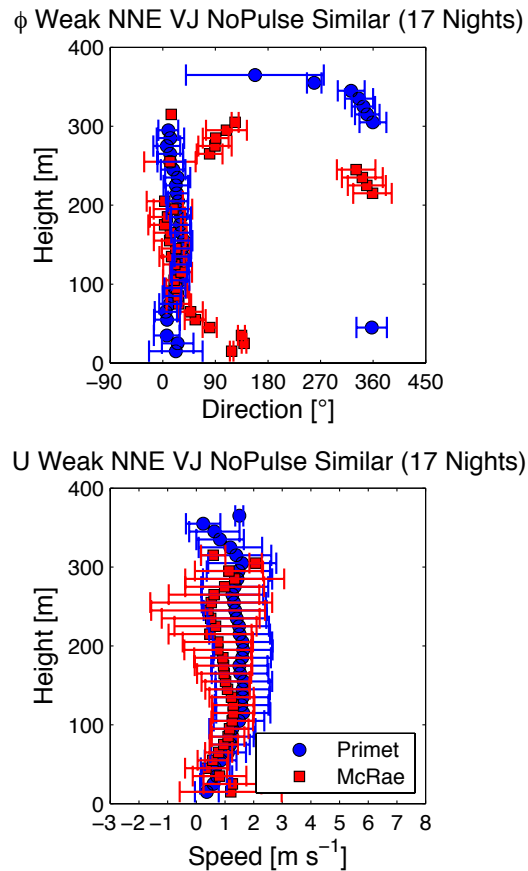


Figure 20: Speed and direction averages by height for Case 1

3.6 Case 2 – Weak SF SW No Valley Jet Pulse Dissimilar

Thirteen nights met the classification criteria for Weak SF, SW flow, No Valley Jet, Pulse Dissimilar. Ensemble-averages for the 13 nights were plotted. (Figure 21). Wind directional averages for these nights are different, with McRae directional averages varying at the lower heights, turning to 280° above 275 m agl. Primet directional averages vary at all heights, but tend towards 275° at higher elevations. The two locations show dissimilar wind speed averages at heights above 130 m agl, with speeds above 1 ms^{-1} and average wind speeds increasing at McRae, while remaining below 2 ms^{-1} at Primet. Wind speed averages increase in variability as height increases, with McRae having larger standard deviation at all elevations.

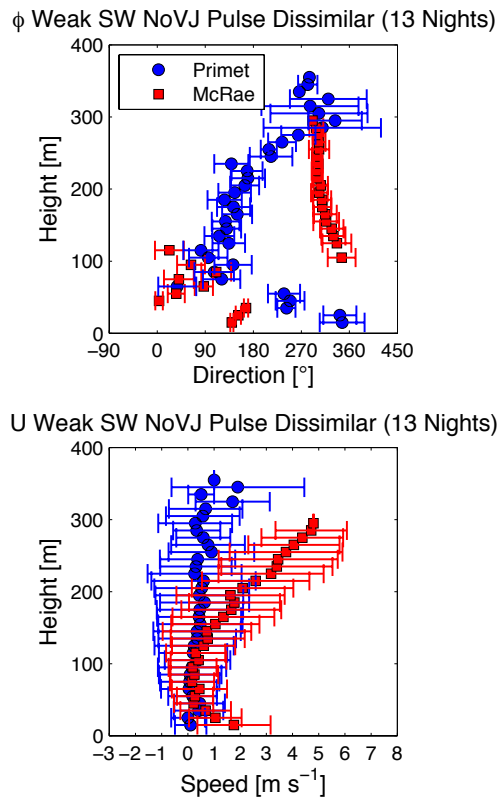


Figure 21: Speed and direction averages by height for Case 2

3.7 Case 3 – Weak SF NNE Valley Jet Pulse Similar

Twelve nights met the classification criteria for Weak SF, NNE flow, Valley Jet, Pulse, Similar, and were also ensemble-averaged (Figure 22). Wind directional averages for McRae and Primet were between 0° and 45° below 295 m agl, shifting to North at gates above 305 m agl. McRae directional averages change from South to North and back to South as height increases. Variability of wind direction averages is small in this case. Both McRae and Primet experience average wind speeds at elevations below 305 m agl as weak, and less than 1.5 ms^{-1} at all gate heights.

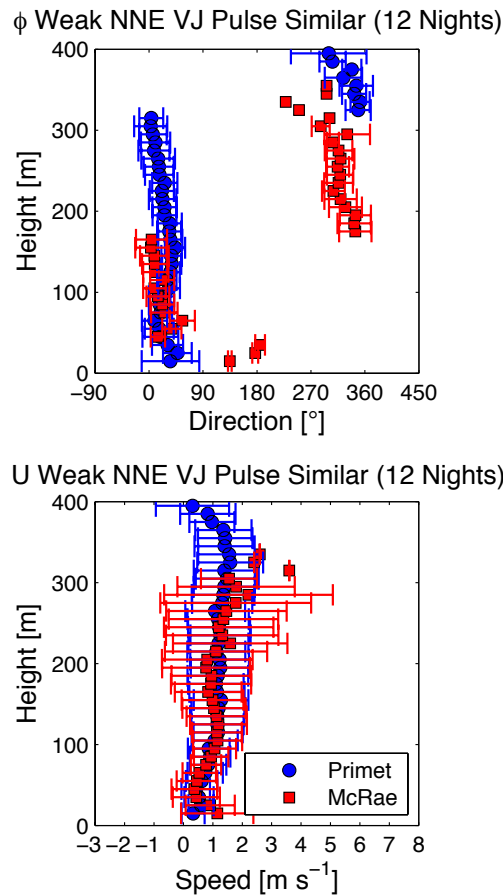


Figure 22: Speed and direction averages by height for Case 3

3.8 Case 4 – Weak SF NNE No Valley Jet Pulse Dissimilar (9 nights)

Nine nights met the classification criteria for Weak SF, NNE flows, No Valley Jet, Pulse, Dissimilar (Figure 23). Wind directional averages were different at the two stations, with McRae shifting extensively at all gate heights while Primet varied at heights below 95 m agl, then averaged Southerly at heights above 115 m agl. Average wind speeds for both stations are below 1 ms^{-1} below 200 m agl. Above 205 m agl, speeds increase steadily to an average of 3 ms^{-1} .

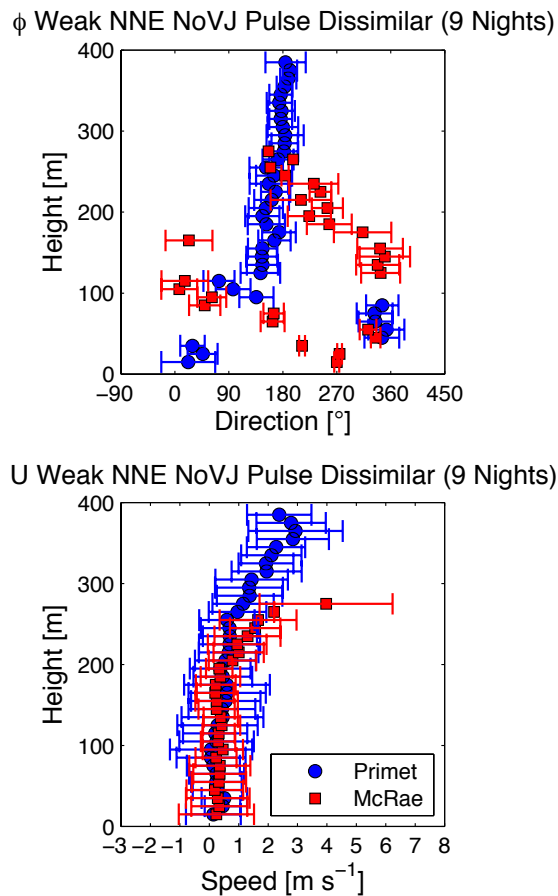


Figure 23: Speed and direction averages by height for Case 4

3.9 Case 5 – Weak SF, SW, No Valley Jet, Pulse, Similar (6 Nights)

Six nights met the classification Weak SF, SW, No Valley Jet, Pulse, Similar (Figure 24). Wind directional averages are approximately 90° different at the two locations. McRae averages South moving to North then back to South as heights increase. Average speeds for both McRae and Primet were relatively similar; however, a weak valley jet was seen at McRae, but not at Primet.

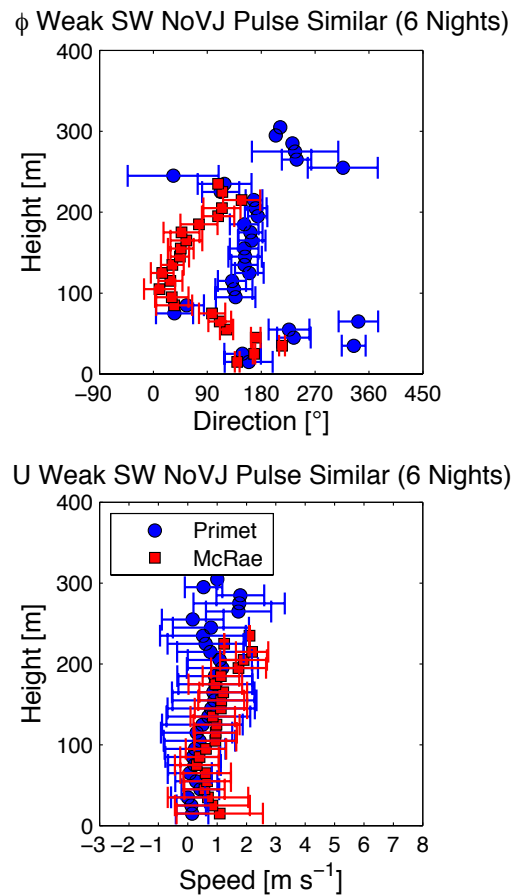


Figure 24: Speed and direction averages by height for Case 5

3.10 Case 6 – Strong SF, SW, No Valley Jet, Pulse, Dissimilar (6 Nights)

Six nights met the classification Strong SF, SW, No Valley Jet, Pulse, Dissimilar (Figure 25). Wind directional averages at McRae are East at the lowest gates, but shift to North at 45 m agl. As height increases, directional averages move from North to East and back to North. McRae varies from North to West and back again, while Primet directions averaged South as height increases. Wind speed averages for McRae were below 1 ms^{-1} at lower gate heights with the exception of the first measurement, 15 m agl. Average speeds increase above 235 m agl to greater than 1 ms^{-1} . Wind speed averages at Primet increase with gate height.

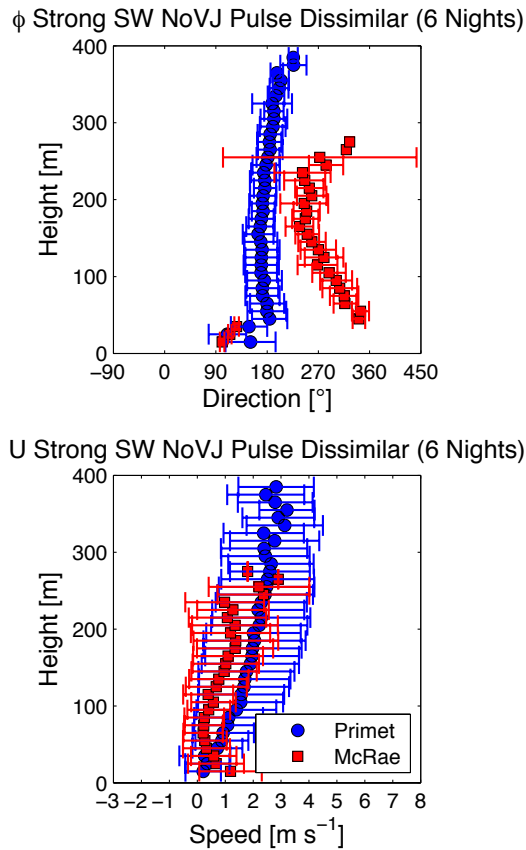


Figure 25: Speed and direction averages by height for Case 6

3.11 Case 7 – Weak SF, SW, Valley Jet, Pulse, Similar (5 Nights)

Five nights met the classification Weak SF, SW, Valley Jet, Pulse, Similar (Figure 26). Directional averages for the two stations were approximately 90° different below 45 meters agl, but were very similar at heights above 55 m agl. Wind speeds at the two locations were relatively similar. A valley jet can be seen at both locations at 105 m agl.

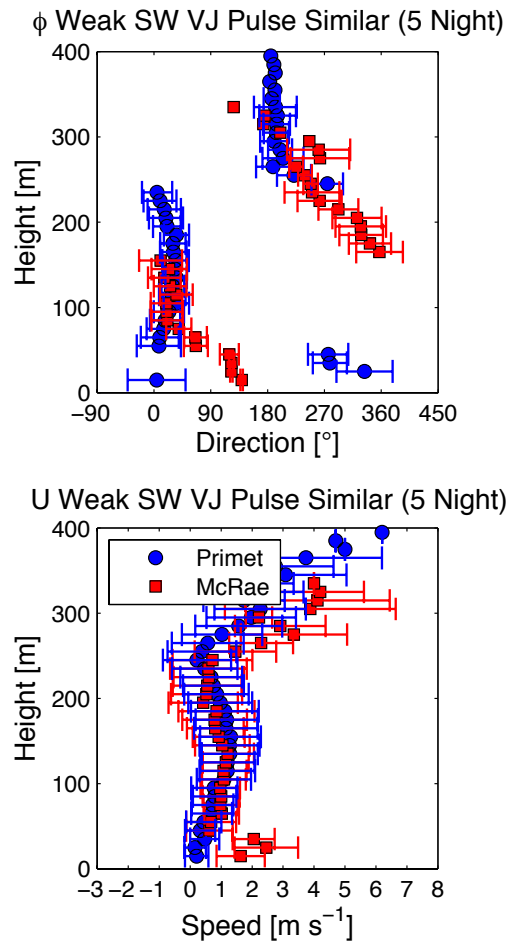
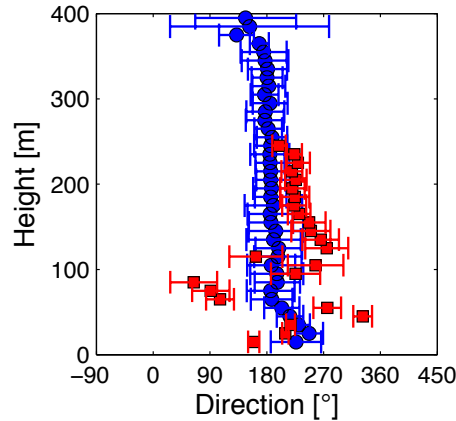


Figure 26: Speed and direction averages by height for Case 7

3.12 Case 8 – Weak SF, SW, No Valley Jet, No Pulse, Dissimilar (5 Nights)

Five nights met the classification Weak SF, SW, No Valley Jet, Pulse, Disimilar (Figure 27). McRae directional averages vary at lower heights, becoming southerly at above 100 m agl and speeds increase steadily above 205 m agl. Primet speed and directional averages were consistent at all heights. Standard deviation indicates variability in speed particularly at lower heights at McRae.

ϕ Weak SW NoVJ NoPulse Dissimilar (5 Nights)



U Weak SW NoVJ NoPulse Dissimilar (5 Nights)

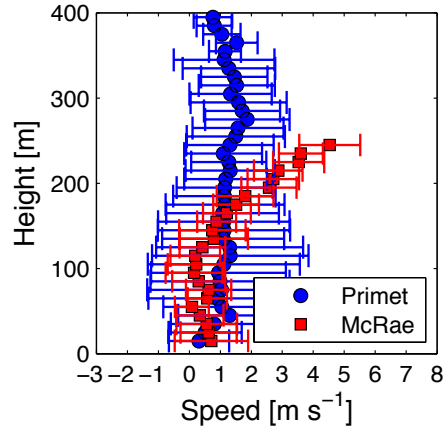


Figure 27: Speed and direction averages by height for Case 8

3.13 Case 9 – Weak SF, NNE, Valley Jet, Pulse, Dissimilar (5 Nights)

Five nights met the classification Weak SF, SW, Valley Jet, Pulse, Disimilar (Figure 28). Directional averages at McRae vary at low heights and becomes similar to Primet above 55 m agl. Average speed for both locations was similar and both stations experience a valley jet at approximately 155 m agl.

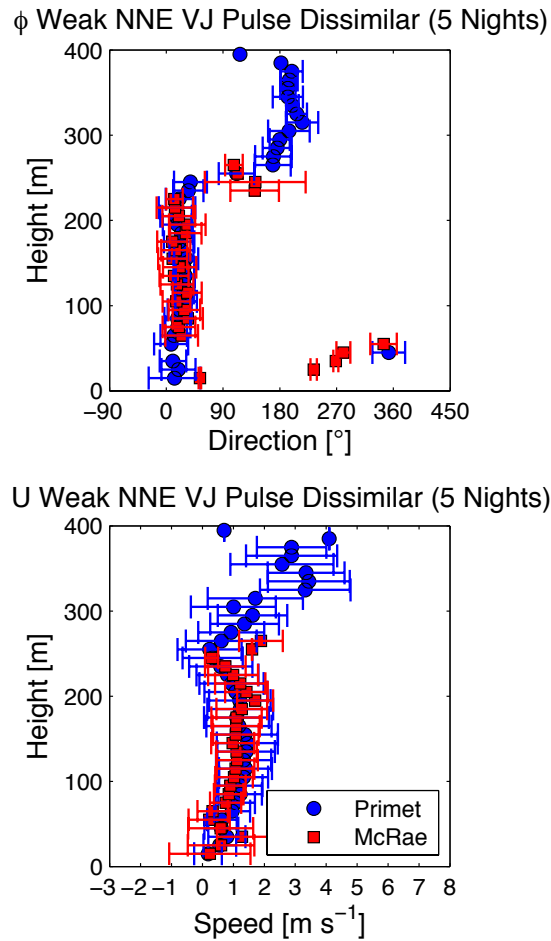


Figure 28: Speed and direction averages by height for Case 9

3.14 Case 10 – Weak SF, SW, Valley Jet, No Pulse, Dissimilar (4 Nights)

Four nights met the classification Weak SF, SW, Valley Jet, No Pulse, Dissimilar (Figure 29). McRae directional averages were East at the first two heights, and then changed to North until 245 m agl, while Primet directional averages vary at low heights. Below 245 m agl, average speeds for both locations were below 1 ms^{-1} except the first McRae gate, which was 2 ms^{-1} . McRae showed a valley jet between 155 and 205 m agl, which was not seen at Primet.

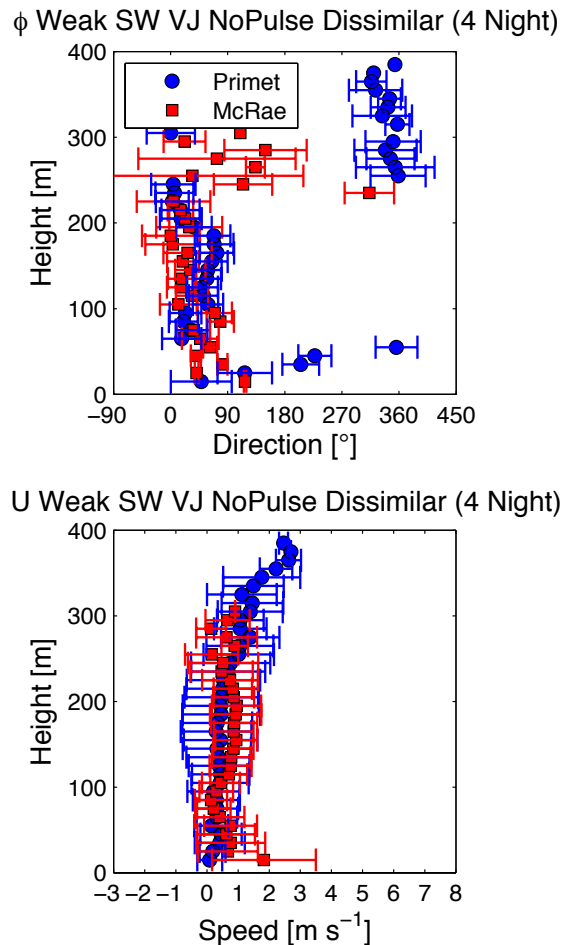
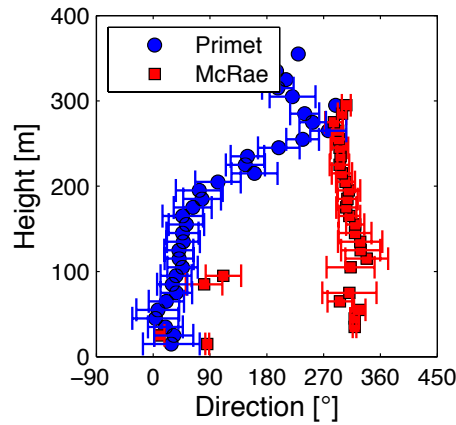


Figure 29: Speed and direction averages by height for Case 10

3.15 Case 11 – Weak SF, NNE, No Valley Jet, No Pulse, Dissimilar (4 Nights)

Four nights met the classification Weak SF, NNE, No Valley Jet, No Pulse, Dissimilar (Figure 30). This case shows variation in both wind speed and directional averages at all heights. Even though only 4 nights met this classification, this is an interesting case because of the very strong flows only at McRae.

ϕ Weak NNE NoVJ NoPulse Dissimilar (4 Nights)



U Weak NNE NoVJ NoPulse Dissimilar (4 Nights)

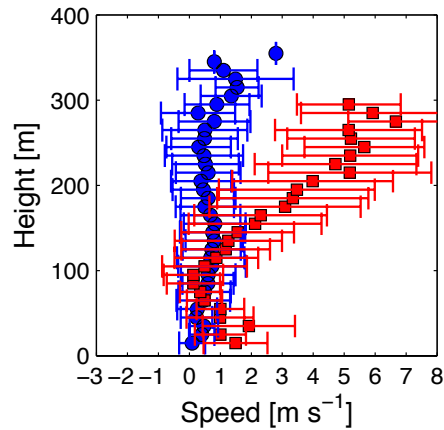


Figure 30: Speed and direction averages by height for Case 11

4 Discussion

As the primary goal of this work was to characterize wind flow within the McRae Valley, we conclude the thesis with a discussion of connectivity and ask whether the methods used (1) appear to be good predictors of connectivity and (2) whether cases could be combined in order to facilitate the characterization of airflow.

Connectivity between McRae and Primet is said to occur when wind flows down the McRae Creek Valley to the Blue River Reservoir. The two SoDAR locations were determined to be connected when both McRae and Primet experienced similar mean wind speed and directional profiles. This occurred most often when the dominant direction was from North-northeast, when wind from the North is able to travel the length of the McRae Creek uninterrupted into Lookout Creek. During periods of weak synoptic direction and dominant wind direction from the Southwest, wind flow within McRae was disconnected at the confluence of the two creeks, McRae and Lookout.

During the study period, the valley was dominated by weak synoptic forcing. Wind direction flows under two dominant regimes, downvalley from the North-northeast, or upvalley from the Southwest. The valley jet was present 49 of the 94 nights. Pulses were present 56 nights, generally when the dominant direction was from the North-northeast. There were 45 nights with similar phenomena at the stations (Table 3).

Table 3: Number of nights meeting each criterion

Criterion	Classification	# Nights	Classification	# Nights
Synoptic Forcing	Weak	79	Strong	15
Wind Direction	SW	42	NNE	52
Valley Jet	Absent	45	Present	49
Pulsing	Absent	38	Present	56
Similar	Similar	49	Dissimilar	45

When combined with the category of Synoptic Forcing, the study period had 38 nights of strong synoptic forcing with flow coming from the Southwest, 14 nights of strong synoptic forcing and flows coming from the North-northeast, 11 nights of weak synoptic forcing with flows coming from the Southwest, and 31 nights of weak synoptic forcing with flows from the North-northeast (Table 4).

Table 4: Number of nights meeting each criterion

Criterion	Classification	# Nights	Classification	# Nights
Strong Synoptic Forcing	SW	38	NNE	14
Weak	SW	11	NNE	31

In the 11 cases evaluated, weak synoptic forcing dominated with only one case showing strong synoptic forcing (Table 5); this demonstrates that the two SoDARs generally experience wind speeds slower than 2 ms^{-1} , so speed is not a good indicator of connectivity. Weak synoptic forcing with wind flow direction from the Southwest occurred in 6 of the 11 cases; however, these cases had fewer nights, 33 of the 94 or 35%. Five cases were classified as weak synoptic forcing with wind flow from the North-northeast, which represents 47 nights or 5% of the nights.

As described above, connectivity was inferred from the classification of the five criteria in 5 of the 11 cases. Of the five criteria, connectivity is most closely related to dominant wind direction, with connection occurring generally when wind direction is from the North-northeast. The large variation in direction that was noted for several cases appears to be due in part to the weak wind regime. There also seems to be a relationship between connectivity of the valleys and the presence of the valley jet, which occurred in every case of valley connectivity and appeared in only one case of non-connectivity. It is also interesting to note that in 3 of the 5 cases where the sodargrams were classified as similar, the valleys appear connected.

The results are noteworthy when the last two criteria, pulsing and similar, are removed (Table 5). In cases 1, 3 and 9, the sodargrams were all classified as weak synoptic forcing with winds from the North-northeast with a valley jet (highlighted in yellow). When these three cases are combined, 35, or 36%, of the nights in the study period were classified the same in the three remaining criteria. What is more interesting is that connectivity within the valley can be inferred in each of these cases. There are two cases of weak synoptic forcing with winds from the North-northeast that were classified as valley jet absent, cases 4 and 11 (highlighted in blue). The two SoDAR locations appeared to be disconnected on these 13 nights, or 14% of the study period.

Of the 5 cases of wind from the Southwest, there were 3 cases of weak synoptic forcing with no valley jet, cases 1, 5 and 7 (highlighted as pink). These three cases, which comprised 19 nights, or 20% of the study period, were

evaluated as disconnected. The two cases of weak synoptic forcing with wind flow from the Southwest with a valley jet, highlighted in blue, comprised 13 nights, or 14% of the study period. For both these cases, the valley was evaluated as disconnected.

Table 5: Connectivity by Case

Case Number	Synoptic Forcing	Flow Direction	Valley Jet	Pulse	Similar	Number of Nights	Valleys Connected
1	Weak	NNE	Yes	No	Yes	17	Yes
2	Weak	SW	No	Yes	No	13	No
3	Weak	NNE	Yes	Yes	Yes	12	Yes
4	Weak	NNE	No	Yes	No	9	No
5	Weak	SW	No	Yes	Yes	6	No
6	Strong	SW	No	Yes	No	6	No
7	Weak	SW	No	No	No	5	No
8	Weak	SW	Yes	Yes	Yes	5	Yes
9	Weak	NNE	Yes	Yes	No	5	Yes
10	Weak	SW	Yes	No	Yes	4	Yes
11	Weak	NNE	No	No	No	4	No

5 Conclusions

5.1 VALCEX and HJA Climate Network Station Data Comparison

With regard to the first objective of this study, the comparison between the SoDAR and the wind cup installed at Primet for the past 20 years, we conclude that the historic wind direction data collected from the propeller anemometer is meaningful and can be used to extend the wind climatology, but the wind speeds cannot be used to investigate the strength of the flows.

5.2 Valley Connectivity

With regard to the second objective of this study, which analyzed the connectivity of the flow within the valley, the valley was considered connected on 88 of the 96 nights classified. The two stations, McRae and Primet experience the criteria synoptic forcing as weak on 79 of the 96 study nights. The second criterion wind direction was classified almost equally at each station; 52 nights were classified as from the North-northeast while 42 nights were classified as from the Southwest. The criterion of valley jet present was determined visually on 49 of the nights. Three of the 5 classification criteria – synoptic forcing, direction and valley jet – were most effective in determining connectivity within the greater McRay - Lookout Creek Valley.

Wind speeds at both McRae & Primet are generally very weak, below 1 ms^{-1} at heights below 195 m agl. Above 205 m agl speeds increase and are generally greater at the McRae station than at Primet; error bars for each gate show variation increasing with elevation. Directional averages show a disconnect between Primet and McRae, with averages at Primet being South at lower elevations and changing to East between 95 and 205 m agl and North-northeast above 205 m agl. At McRae, on the other hand, flows above 45 m agl and below 105 m agl vary between South and West, moving to from the West between 115 and 305 m agl; above 305 m agl, flows again vary between South, Southeast and North. Near zero wind speed variation, shown by error bars, is the result of opposing flows with similar magnitude, so the resultant vector speed is near zero.

5.3 Cases based on 5 Classification Criteria

Of the 5 criteria used to classify each sodargram of a night of the study period two – flow direction and valley jet – were most effective in determining connectivity within the McRae Valley, given that weak synoptic forcing dominated the study period. The classification of Synoptic Forcing would be effective if the valley were not dominated by weak winds.

The problem was essentially a classification problem. Could the 96 daily sodargram analyses by 3, 4 or 5 criteria be input to a machine-learning tool, to produce algorithms that would correctly analyze sodargrams of other topographically similar locales? Or is a classification based on a visual review of the raw data in the form of a sodargram effective? While the study may have been more robust had the researcher used multiple visualization techniques, it is apparent that 3 of the 5 criteria were effective as determining connectivity.

6 Future Work & Recommendations

This study may have been more robust had the classification criteria been limited to two or three phenomena: synoptic forcing and dominant wind direction, with possible inclusion of the valley jet. Limiting the number of phenomena classified would generate fewer cases, which would create a stronger relationship between phenomena and valley connectivity. Further, a smaller number of phenomena evaluated might have allowed for multiple evaluations of the sodargrams, which in turn would have allowed for a comparison of each

evaluator's set of evaluations. Such an analysis might strengthen the validity of the visual classification process.

Wind direction variability typically accompanies weak winds. The classification of wind direction was limited by using only two dominant directions, NNE and SW. Using four directional categories – NW, NE, SW, and SE – would allow for classifying sodargrams with wind directions not easily grouped into NNE or SW. It would be interesting to evaluate how many of the 94 nights of the study period were not easily classified into NNE or SW.

The next step in this study would include analysis of multiple visualization techniques. Perhaps comparing the visual analysis of sodargrams to windroses, or other visualization tools. A study of that type could be extremely interesting in determining which methods of visualization most effectively display and communicate this data-rich information. Previous work for the Visualizing Terrestrial and Aquatic Systems (VISTAS) project resulted in reviewing hundreds of visualizations from four hydrology journals (Cushing et al., 2012). During that review, visualizations and modeling software used by hydrologists were noted with interest. It would be extremely helpful and telling to input the Primet and McRae daily and aggregated data into tools that could portray the physical phenomena (wind direction and speed) in three dimensions superimposed onto the topographic surface, and animate these data through time. It would be interesting to explore how visualization techniques used in other disciplines, such as hydrology, that also study fluids in motion could be used to visualize (then

characterize and qualitatively or quantitatively analyze) micrometeorological phenomena.

7 Bibliography

- Arya, P. S. (2001). Introduction to micrometeorology. London, Academic Press.
- Clements, C. (2002). "Cold-Air-Pool Structure and Evolution in a Mountain Basin: Peter Sinks, Utah." Journal of Applied Meteorology and Climatology **42**.
- Cushing, J., E. Hayduk, J. Walley, L. Zeeman, N. Stevenson-Molnar, K. Winters, D. Lach, M. Bailley, B. J. Bond, J. Bolte, C. K. Thomas and S. Stafford (2012). How Ecologists 'Visualize' Research in Publications: VISTAS Project Ecology Journal Survey. Poster presented at Ecological Society of America Annual Meeting. Portland, Or., Ecological Society of America.
- Dorninger, M., C. D. Whiteman, B. Bica, S. Eisenbach, B. Pospichal and R. Steinacker (2011). "Meteorological Events Affecting Cold-Air Pools in a Small Basin." Journal of Applied Meteorology and Climatology **50**(11): 2223-2234.
- Folken, T. (2008). Micrometeorology. Verlag Berlin Heidelberg, Springer.
- Lundquist, J. D., N. Pepin and C. Rochford (2008). "Automated algorithm for mapping regions of cold-air pooling in complex terrain." Journal of Geophysical Research **113**(D22).
- Mahrt, L. (2008). "Mesoscale wind direction shifts in the stable boundary layer." Tellus Series A-Dynamic Meteorology and Oceanography **60A**: 700-705.
- Mahrt, L., S. Richardson, N. Seaman and D. Stauffer (2010). "Non-stationary drainage flows and motions in the cold pool." Tellus A: no-no.
- Mayer, J.-C. (2005). Characterization of the atmospheric boundary layer in a complex terrain using SODAR-RASS. Master of Science in Geoecology, University of Bayreuth.
- Smith, S. A., A. R. Brown, S. B. Vosper, P. A. Murkin and A. T. Veal (2009). "Observations and Simulations of Cold Air Pooling in Valleys." Boundary-Layer Meteorology **134**(1): 85-108.
- Smoot, A. R. (2012). Linking dynamics of the near-surface flow to deeper boundary layer forcing in the nocturnal boundary layer. Masters of Science, Oregon State University.
- Thomas, C. K., A. M. Kennedy, J. S. Selker, A. Moretti, M. H. Schroth, A. R. Smoot, N. B. Tufillaro and M. J. Zeeman (2012). "High-Resolution Fibre-Optic Temperature Sensing: A New Tool to Study the Two-Dimensional Structure of Atmospheric Surface-Layer Flow." Boundary-Layer Meteorology **142**(2): 177-192.
- Whiteman, C. D. (1990). "Observations of thermally developed wind systems in mountainous terrain." Atmospheric processes over complex terrain, Meteor. Monogr **23**(45): 5-42.

- Whiteman, C. D. and S. Zhong (2008). "Downslope Flows on a Low-Angle Slope and Their Interactions with Valley Inversions. Part I: Observations." Journal of Applied Meteorology and Climatology **47**(7): 2023-2038.
- Whiteman, C. D., S. Zhong, W. J. Shaw, J. M. Hubbe and Z. Bian (2001). "Cold Pools in the Columbia Basin." Weather and Forecasting **16**.

